energies

MDPI

Article

Present Geothermal Characteristics and Influencing Factors in the Xiong'an New Area, North China

Sasa Guo [1,2], Chuanqing Zhu [1,2,*], Nansheng Qiu [1,2], Boning Tang [1,2], Yue Cui [1,2], Jiatang Zhang [1,2] and Yuhang Zhao [1,2]

[1] State Key Laboratory of Petroleum Resources and Prospecting, China University of Petroleum, Beijing 102249, China; gss61333@163.com (S.G.); qiunsh@cup.edu.cn (N.Q.); tangboning@foxmail.com (B.T.); yueyuxinfei1995@163.com (Y.C.); 18810600295@163.com (J.Z.); zhaoyuhang1230@gmail.com (Y.Z.)

[2] College of Geosciences, China University of Petroleum, Beijing 102249, China

* Correspondence: zhucq@cup.edu.cn

Received: 3 September 2019; Accepted: 6 October 2019; Published: 14 October 2019

Abstract: The present geothermal characteristics and influencing factors are analyzed to conduct geothermal resource exploration in the Xiong'an New Area. Thermal conductivity data for 100 rock samples are obtained from different wells and a sedimentary strata thermal conductivity column is proposed. From these data, heat flow distribution in the area is mapped using equilibrium temperature logs obtained for 32 wells. The heat flow in this area is found to be 53.3–106.5 mW·m^{-2} (average: 73 mW·m^{-2}). The uplift heat value in Niutuozhen and Rongcheng uplift is 106.5 and 90 mW·m^{-2}, respectively. The sag heat flow is relatively low and the Baxian sag's heat flow value is 48.9–61.6 mW·m^{-2}. Thermal conductivity differences among Cenozoic caprock, Proterozoic carbonate reservoirs, and basement rock mainly affects the geothermal distribution. The low and high thermal conductivities of the caprock and thermal reservoir as well as basement, respectively, cause heat flow redistribution in the surface during conduction. Groundwater rises to geothermal reservoirs through heat-controlling faults, causing convective heat transfer and increasing the geothermal reservoir temperature; therefore, high-temperature groundwater accumulates in the shallow uplift areas. The caprock's thin uplift area exhibits a high geothermal background due to water convergence. Understanding the geothermal characteristics and influencing factors is necessary for understanding the distribution law and factors influencing geothermal resources and guiding geothermal exploration and development in the Xiong'an New Area.

Keywords: geothermal gradient; terrestrial heat flow; rock thermal conductivity; geothermal resources; Xiong'an New Area

1. Introduction

The geotemperature of a sedimentary basin embodies the present thermal state of the basin and is controlled by the deep lithosphere thermodynamic processes and tectonic evolution of the shallow basin. Geothermal gradient, terrestrial heat flow, thermal conductivity, and radioactive heat production are important evaluation parameters for geothermal research and resource exploration [1–3]. Many factors, such as fault zones [4], regional structure, magmatic activity, and groundwater activity, affect the geothermal field.

Faults mainly act as heat transfer channels, resulting in local geothermal anomalies because the Miocene fault activity significantly influences the geothermal field [5]. Different tectonic forms, such as uplifts and depressions, caused by the tectonic movements change the horizontal and vertical thermal conductivity of rocks, refracting and redistributing the heat flow to gather in uplifts [6–9]. The thermogenesis from magmatic activity, especially the Cenozoic magmatic activity, affects the

regional geothermal fields [8] with younger magma activities having a larger scale and more retained residual heat, considerably affecting geotemperature. Groundwater activity is an important factor affecting geotemperature distribution. In runoff areas with cold groundwater, geotemperature usually exhibits a negative anomaly, whereas the geotemperature anomalies are often positive in hot water discharge areas [10].

Xiong'an New Area, a state-level new area, which is located in the hinterlands of Beijing, Tianjin, and Baoding, was established by the Chinese government in 2017. Since this area is rich in geothermal resources in the middle and eastern part of China and have the best development and utilization conditions, it is a typical demonstration area for geothermal development. Currently, Xiong'an New Area is building a world-class transparent digital platform and global model for geothermal resource utilization. This area exhibits favorable geothermal and geological conditions; therefore, it is a key geothermal exploration area. The exploration of the geothermal field characteristics and influencing factors of this area was initiated in the 1980s. Previous studies discovered underground hot water when exploring the Niutuozhen uplift, and the basic understanding of this area was obtained by studying the reservoir types and genetic model and patterns of geothermal resource. The area is a medium–low-temperature geothermal resource, with energy mainly being transferred through heat conduction. Previous studies have conducted preliminary analysis of the temperature field in this area [11–16]. Zhou [17] attributed the shallow geothermal field characteristics of the North China Plain to deep groundwater activities under a geothermal background determined by geological structures. Based on the consistency of the geothermal gradient and geological structure distribution, Chen et al. [11,12] inferred that under the tectonic framework of the North China Basin, the rock thermal property differences in the transverse and longitudinal directions were the main controlling factors of present distribution.

Recent thermometry studies [14,18,19] have deepened the understanding of the geothermal gradient and geothermal heat distribution characteristics of the area and have revealed that the planar distribution of geothermal gradient and heat flow correspond well with the basement relief. From the viewpoint of the formation mechanisms of the Xiong'an New Area geothermal fields, some researchers [15,16] have introduced a qualitative understanding that the geothermal field formation exhibits an important relation with the geological structures, high-temperature geothermal water through multiple karst and fissure spaces in reservoirs, and heat convection occurs through faults and uplifts due to the favorable insulation conditions of the Quaternary caprocks.

Previous geotemperature studies in the Xiong'an New Area have mainly investigated the geothermal field distribution characteristics; however, comprehensive analysis of the factors that control the geothermal fields has not been sufficient. Therefore, based on previous studies this study considers 100 new measured rock thermal conductivity data, systematically analyzes the current heat flow distribution and geothermal field characteristics, and discusses main factors affecting the geothermal field. The proposed study has an important reference value in understanding the geothermal field formation mechanisms and exploring and developing geothermal resources.

2. Geological Background

The Xiong'an New Area is in the Jizhong Depression of the North China Basin (Figure 1a). The North China Basin is a Mesozoic–Cenozoic downfaulted basin in the North China platform and has undergone several tectonic movements since the Archaean, forming a series of NE, NWW, and WE tensional faults (Figure 1b). During the Early Tertiary, a series of fault depressions and uplifts were formed under strong extension, resulting in an interphase tectonic system with uplifts and sags. Subsidence was dominant from late Tertiary to Quaternary, forming the uplifts and sags of the interphase tectonic system [12].

The thermal evolution of the North China Craton remained stable after the Early Mesozoic. Since the Mesozoic, the thermal state and properties of the lithosphere in the eastern part changed, experiencing two heat flow peaks (85–88 $mW \cdot m^{-2}$) [20]. The subduction of the Pacific Plate, together

with deep mantle convection since the Late Mesozoic, and crustal thickening and strike-slip pull apart tectonic setting caused by the collision between the Eurasian and Indian plates since the Cenozoic resulted in the North China Basin appearing as a high heat-flow area, with a present heat flow of 60–68 mW·m^{-2} [21,22].

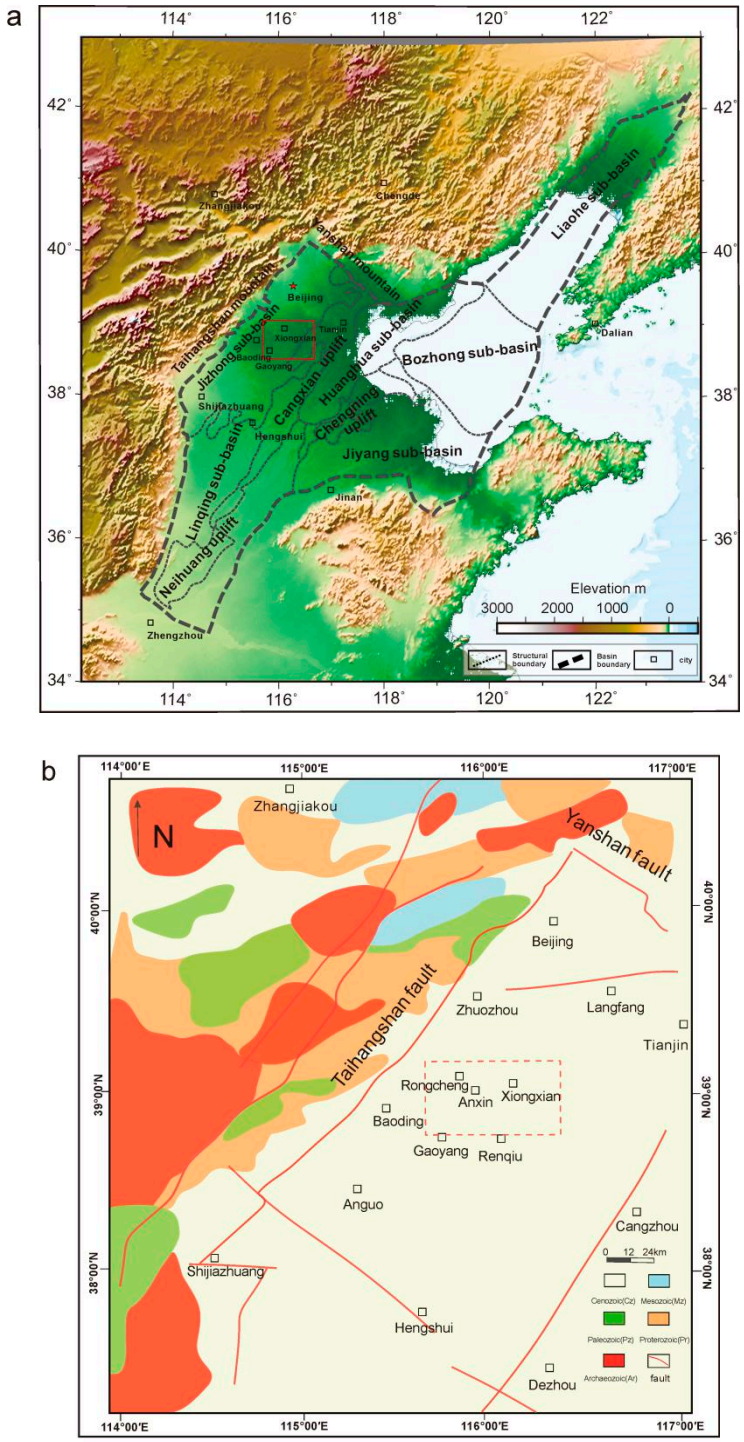

Figure 1. Structural unit divisions and stratigraphy distribution characteristics of the Xiong'an New Area (subfigure a adapted from Qiu [20]). Geotectonic location and regional geological map of the Xiong'an New Area (**a**); Stratigraphy and geological distribution characteristics of the Xiong'an New Area (**b**).

The Jizhong Depression is a Mesozoic–Cenozoic deposit developed on the basement of the North China platform with a NE–SW strike. It is surrounded by the Yanshan, Xingheng, Taihangshan, and Cangxian uplift to the north, south, west, and east, respectively. In the Jizhong Depression, the current geothermal gradient at a depth of 3000 m is 20.8–41.0 °C/km with an average of 31.6 °C/km and terrestrial heat flow is 48.7–79.7 mW·m^{-2}, both of which have a west-to-east increasing trend. The planar distribution corresponds well with the basement topographic relief [23]. The geothermal gradient and temperature of the Niutuozhen uplift are high, whereas they are low in the Langgu and Baxian sags. The Xiong'an New Area is in the Jizhong Depression, and the tectonic unit includes three uplifts, i.e., the Rongcheng, Gaoyang, and Niutuozhen uplifts, and three sags, i.e., the Baxian, Raoyang, and Baoding sags.

The North China Basin underwent the following tectonic evolution: the formation period of the metamorphic crystalline basement was from the Archean to Paleoproterozoic; there were three stages of fault-depression development from the Meso–Neoproterozoic to Neogene; and the North China Basin entered a stable sedimentary stage since the Neogene. During the late Jurassic, the subduction of the Kula Plate to NNW caused the North China Basin exhibit a NE-to-NNE tectonic framework. Three stages of fault-depression evolution led the tectonic features to be interphased with faults and depressions, forming multiperiod faulted depression stacked basins [13,24]. The area's stratigraphic column (Figure 2b) shows four layers of geothermal reservoirs, i.e., the Nm formation of the Neogene, Guantao formation of the Neogene, Gaoyuzhuang formation of the Jixian system, and Jxw Formation of the Jixian system.

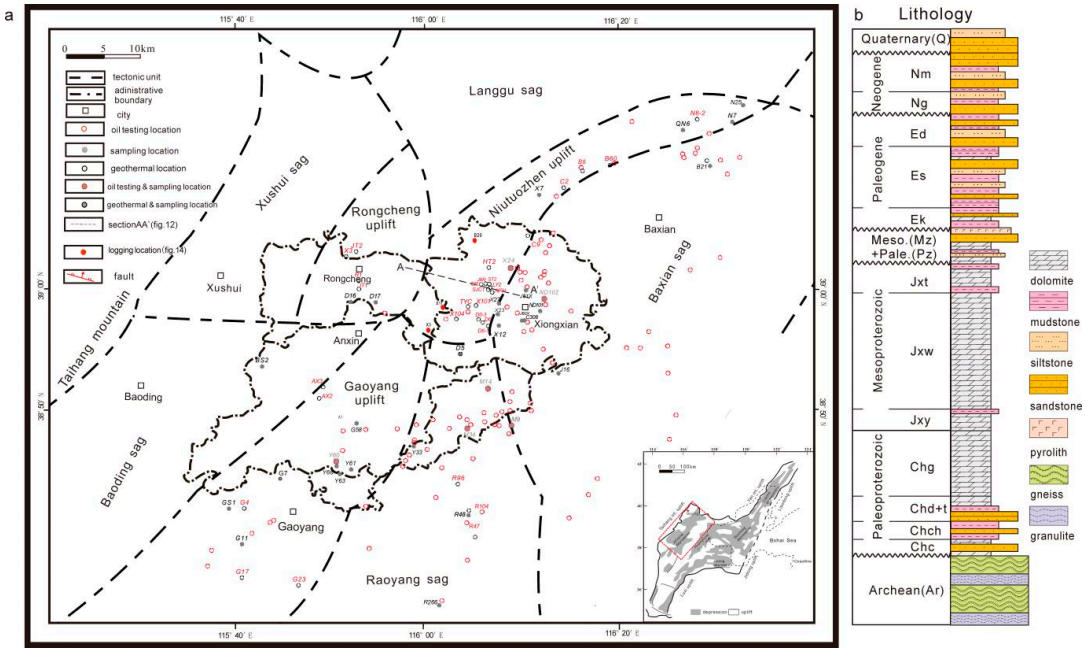

Figure 2. Tectonic and well locations (**a**) and stratigraphy (**b**) of the Xiong'an New Area.Geological structure and distribution of sampling points and well locations in Xiong'an New Area (**a**); The main lithlogic stratigraphy column in Xiong'an New Area (**b**).

The Jxw Formation's geothermal reservoirs mainly comprise dolomite and calcite dolomite and are characterized by wide distribution, shallow burial, high temperature, large reserves, and excellent water quality [25]. This formation has a high mining value (high temperature and rich water) and currently holds the key in the development of geothermal resources. The Cenozoic strata mainly consist of sand and mudstone, which is a good heat storage barrier with low thermal conductivity.

3. Present Geothermal Field

3.1. Geothermal Temperature Data of Boreholes and Oil Testing

The borehole temperature data mainly include the measurement data of stationary-borehole temperature, static-well temperature, oil-testing temperature, and nonstationary-borehole temperature.

To study the sedimentary basin geothermal characteristics, the system steady-state temperature measurements and oil-testing temperature data are considered to be the most reliable. This study collected temperature data from 13 geothermal [19,26] and 19 oilfield wells [23] in the study area, obtaining the geothermal gradient for each by temperature–depth linear fitting (Figures 3 and 4).

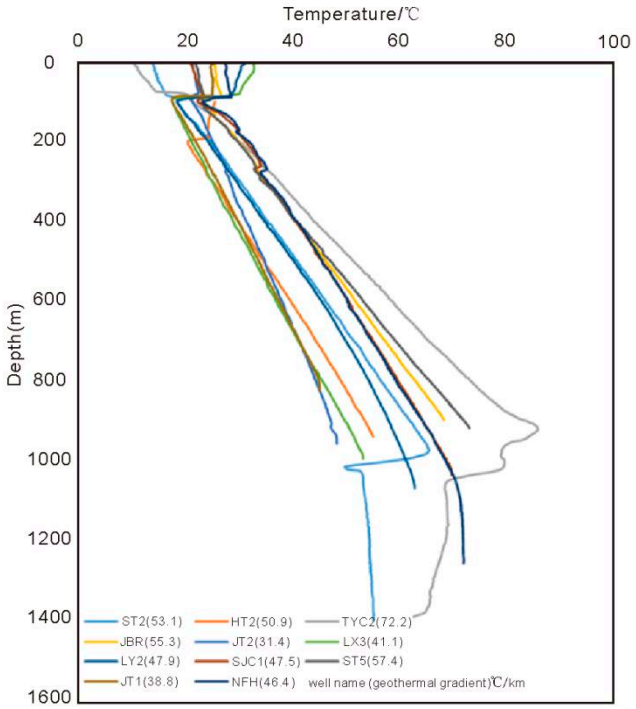

Figure 3. Temperature–depth graph of the geothermal wells in Xiong'an New Area (adapted from Li [14]). The temperature-measurement depths are as follows (m): ST2 (400–1000); HT2 (400–900); TYC2 (300–800); JBR (400–800); JT2 (300–800); LX3 (300–800); LY2 (300–800); SJC1 (400–800); ST5 (300–800); and JT1 (300–800). The measurement depths exhibit steady-state conduction.

As shown in Figures 3 and 4, the temperature logging data of several wells can be clearly divided into an upper section with a conductive temperature curve without any groundwater activity interference and lower section with a convective temperature curve (e.g., ST2, TYC2, and NFH1). Majority of the conductive temperature curves are distributed in the Cenozoic strata and are shallow, and the convective temperature section mostly corresponds to the Proterozoic dolomite thermal reservoir. For example, the D6 well (Figure 5) is in the Quaternary Nm formation above 1200 m, which has a main lithology of sandstone and mudstone exhibiting poor heat transfer performance and is mainly in the heat conduction mode. Below 1200 m, the D6 well is in the Jxw Formation, which mainly has a dolomite lithology, and can be expressed by the convection temperature curve.

There are 30 systematic temperature logging wells in the Xiong'an New Area, majority of which are in the uplift areas (borehole locations in Figure 2a). Only R47, R96, R104, and C9 wells are located in the depression areas and have geothermal gradients of 29.4 °C/km–38.1 °C/km, with an average of 33.3 °C/km. All the remaining wells are located in the uplift areas and have geothermal gradients ranging 34.9 °C/km–72.8 °C/km, with an average of 48.3 °C/km, which is significantly higher than the wells in the depression areas and exhibits an abnormally high geothermal field.

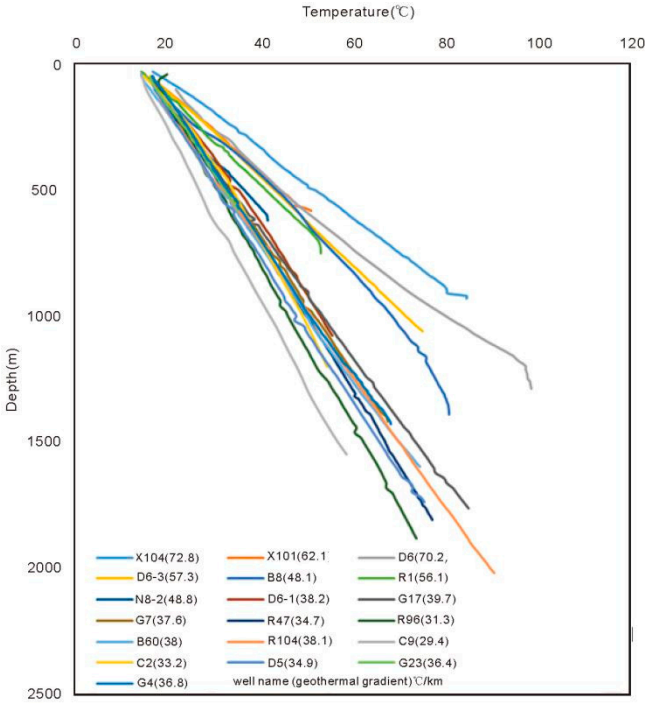

Figure 4. Temperature–depth graph of oilfield wells in the Xiong'an New Area (adapted from Chang Jian [18]).

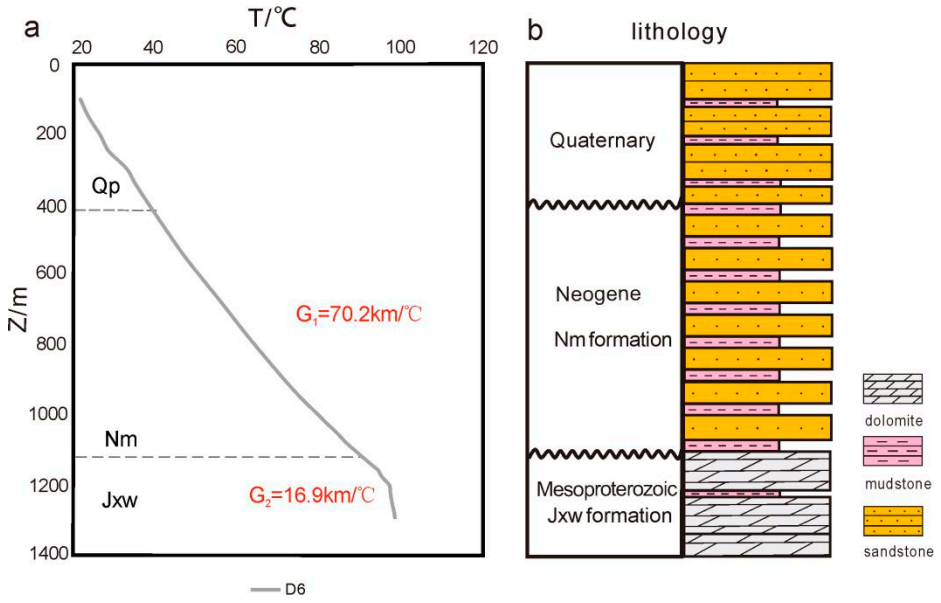

Figure 5. D6 well temperature profile (**a**) and the formation lithology column (**b**).

The oil-testing temperature refers to the temperature data obtained by testing oil and pressure in the oil-bearing strata of production or exploration wells. The oil-testing temperature data can reflect the geothermal temperature distribution characteristics in the basin. This study collected 100 oil-testing data [18,23] (Figure 6) published by previous research in the study area. The well locations are distributed in various parts of the Xiong'an New Area. The temperature logging depths were 795–4637.5 m and geotemperature was 56 °C–182.7 °C. The temperature generally varies linearly with depth; however, there are some abnormal values that deviate from the straight line. The oil-testing data have an average geothermal gradient of approximately 27.8 °C/km. Furthermore, the uplift and sag oil-testing data are separated, with the uplift data basically falling above the trend line, indicating a

higher geothermal gradient value with an average value of approximately 39.9 °C/km. On the contrary, the depression oil-testing data fall below the trend line, indicating a low geothermal gradient, with an average of 29.9 °C/km. The geothermal field characteristics of the oil-testing data are consistent with those of the temperature logging data.

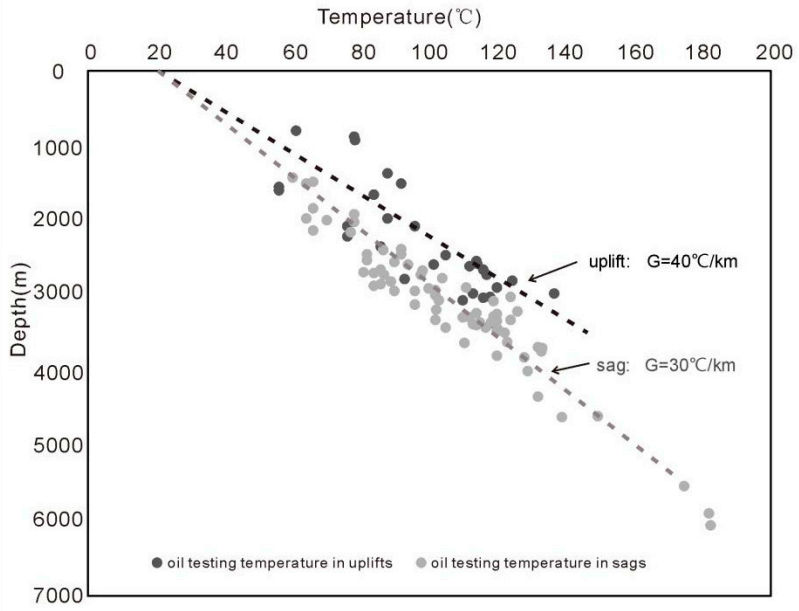

Figure 6. Schematic of the oil-testing temperature data.

3.2. Geothermal Gradient Distribution in Caprocks

Geothermal gradient is an important parameter for studying the geothermal state of the basin. Based on a previous analysis, caprock lithology is dominated by sand and mudstone, whereas the reservoir is dominated by dolomite and limestone [14]. Groundwater activity is strong in geothermal reservoirs, disturbing the geothermal field; therefore, a regular change in temperature with depth is not reflected. The geothermal gradient of the caprock was obtained on the basis of the oil-testing and system temperature data.

Figure 7 shows a planar map of the geothermal gradient obtained in the area. The Xiong'an New Area has a high geothermal background, with a caprock geothermal gradient of 24.6 °C/km–72.8 °C/km with an average of 35 °C/km. This geothermal gradient is slightly greater than that observed in the Mesozoic–Cenozoic rifted basins of eastern China and is significantly higher than those of the Ordos Basin (24.4 °C/km) [2,27] and Tarim Basin (20 °C/km) [28]. The caprock geothermal gradient shows obvious planar distribution characteristics. All the uplifts show geothermal abnormalities, with the Niutuozhen uplift having the highest geothermal gradient at 50.9 °C/km–57.4 °C/km, with an average of 54.5 °C/km, whereas the Rongcheng and Gaoyang uplifts have gradients of 38.8 °C/km–56.5 °C/km and 32 °C/km–39.7 °C/km, respectively, with respective averages of 44.8 °C/km and 36.3 °C/km. In comparison with the uplifts, the sags exhibit lower geothermal gradients, with the Baxian and Raoyang sags having geothermal gradients of 25.7 °C/km–33.9 °C/km and 27.9 °C/km–37.0 °C/km, respectively, with respective averages of 29.4 °C/km and 32 °C/km. In general, the Xiong'an New Area's geothermal gradient is consistent with respect to the basement relief, and the west–east geothermal gradient trend is low–high–low–high–low, which corresponds to the interphased uplift and depression tectonic pattern [18,26].

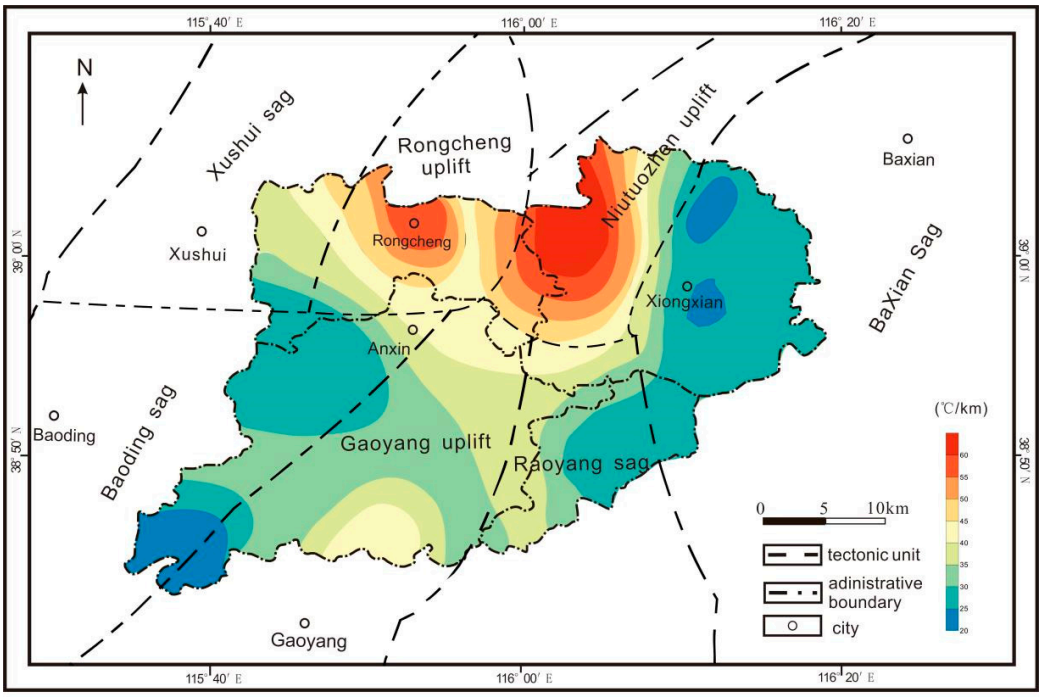

Figure 7. Planar graph of the geothermal gradient in the Xiong'an New Area.

3.3. Top Surface Temperature Distribution Characteristics of the Jxw Formation

The top depths of the Jxw Formation (Figure 8) show large differences throughout the Xiong'an New Area, with depths of 764–5987 m. The top depths of the Rongcheng and Niutuozhen uplifts are relatively low, within 764–2000 m; the minimum depth is in the Niutuozhen uplift, with an average of 1200 m. The average top buried depth in the Rongcheng uplift of the Jxw Formation is approximately 1300 m. The top depth of the reservoir in the Raoyang and Baxian sag is relatively high, within 2500–5987 m, with the maximum of 5987 m being observed in the Baxian sag. The maximum top depth in the Raoyang sag is 4931 m, with an average of 4300 m. The top depth of the Gaoyang uplift is medium, with an average of approximately 3000 m.

Based on the obtained geothermal gradient and known top depth in the Jxw Formation, the authors calculated the top surface temperature for each well in the Jxw Formation as follows:

$$T = GZ + To, \quad (1)$$

where To (°C) is the temperature at the constant temperature zone (set at 14 °C), Z is the depth (m), G (km/°C) is the geothermal gradient of the sedimentary layer and T (°C) is the temperature at a depth of Z (m).

Therefore, the top surface temperature distribution of the Jxw Formation in the Xiong'an New Area can be obtained as shown in Figure 9.

The reservoir top temperatures in the Xiong'an New Area vary with different structural units. The top depths of the thermal reservoir in the Rongcheng and Niutuozhen uplifts are relatively low, with an average depth of approximately 1200 m and top temperatures of 40 °C–90 °C, indicating an increase from north to south. The average geothermal reservoir top depth of the Gaoyang uplift is approximately 3000 m and its top temperature is high, i.e., 90 °C–135 °C, with an average temperature of 110 °C, increasing from north to south. The temperatures in the Baxian and Raoyang sag are high, with the highest value being observed in the latter, denoting an increasing northwest-to-southeast trend. The temperature is higher in the southeast, reaching up to 141 °C; however, the geothermal reservoir is buried deep at approximately 4300 m. In general, the geothermal conditions in the Rongcheng and

Niutuozhen uplifts are feasible as high-temperature water is obtained in shallow areas, followed by the Gaoyang uplift, Baxian sag, and Raoyang sag.

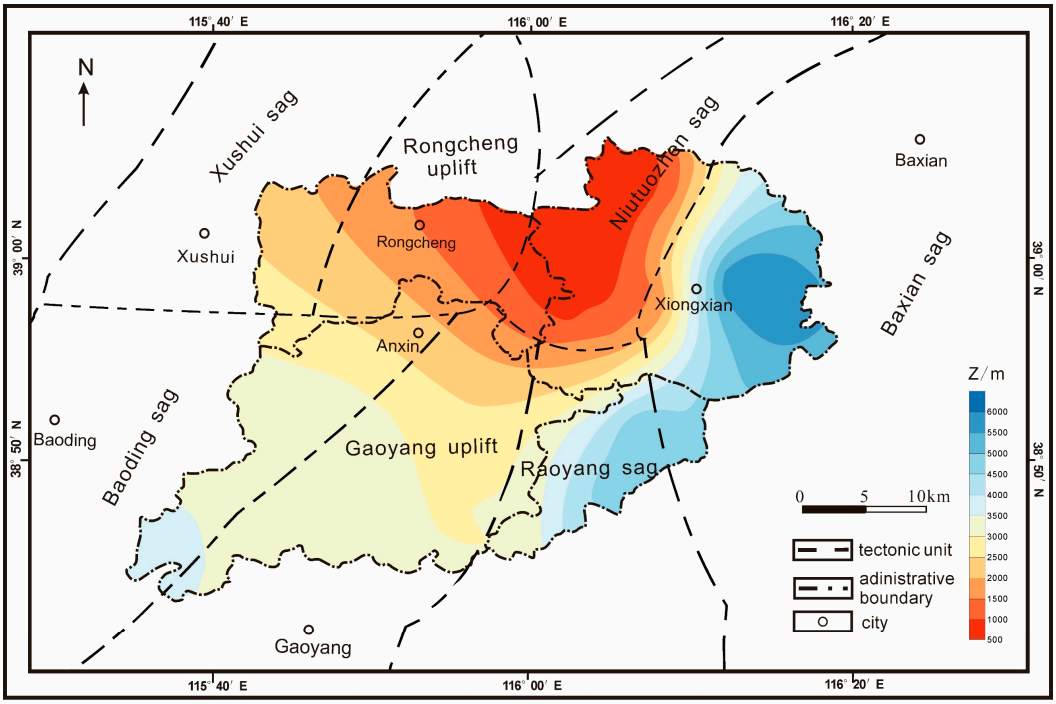

Figure 8. Top depth of the Jxw Formation in the Xiong'an New Area.

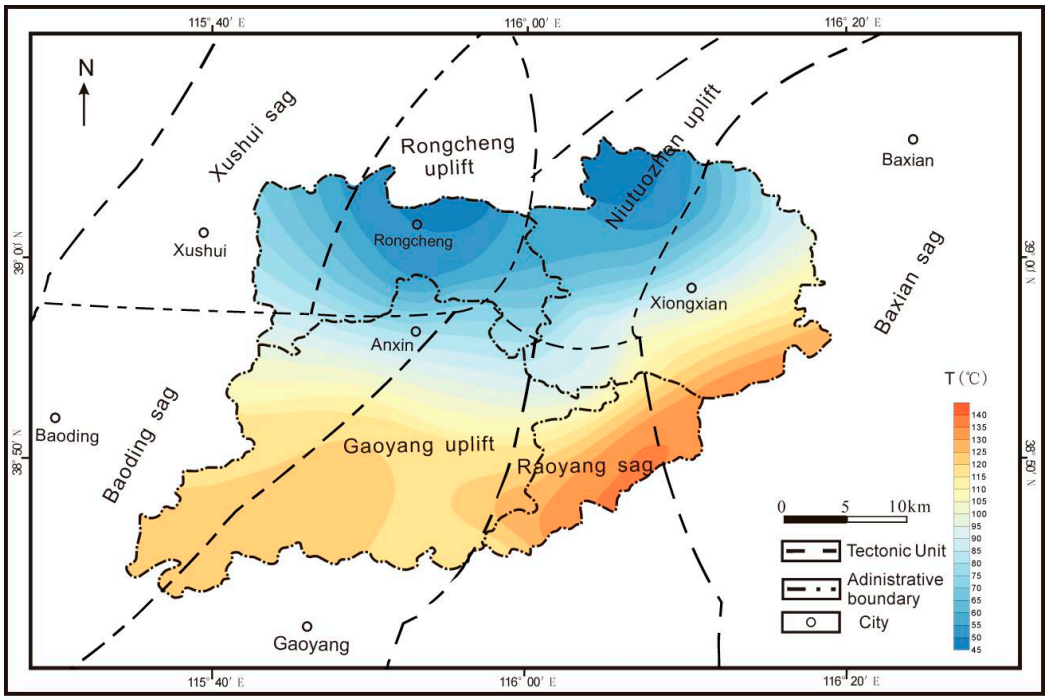

Figure 9. Calculated top surface temperature distribution of the Jxw Formation in the Xiong'an New Area.

3.4. Distribution Characteristics of the Current Geothermal Heat Flow in the Xiong'an New Area

Geothermal heat flow is the most direct expression of thermodynamic processes occurring in the interior of the Earth and is closely related to the geothermal gradient and thermal conductivity of

rocks. Geothermal heat flow can also reflect the regional geothermal field characteristics accurately than other geothermal parameters. Therefore, it is an important parameter for studying the geothermal fields, regional thermal state, and thermal background, as well as for the exploration and evaluation of geothermal resources [8,29,30]. The K parameter of rock thermal conductivity reflects the rock thermal conductivity and is of great significance in the basic geological research of Earth's deep thermal state, lithospheric thermal structure, and thermal evolution [31]. The K parameter is also important for heat flow calculation and lithospheric thermal structure simulation as well as for investigating the current thermal state of the crust [22].

The 100 samples measured in this study were obtained at sampling depths of 778–5325 m from 33 wells located in different areas of the Xiong'an New Area and covering the main strata and lithologies from the Archaean to the Cenozoic.

The thermal conductivity measurements were conducted at room temperature (20 °C) and normal atmospheric pressure using a Hot Disk thermal constant analyzer (Hot Disk AB, Goteberg, Sweden), with a measurement range of 0.03–500 W/(m·K) and ±3% accuracy.

The hot disk analyzer (Figure 10) measurement is based on the principle of a transient flat heat source method. The core element is a thin-layered, disc-shaped, temperature-sensitive probe, which comprises a conductive nickel metal foil and continuous double helix sheet. During testing, a constant output current is passed through the probe. The resistance of the probe changes with an increase in the temperature. The different thermal conductivities of the samples result in different heat losses of the probe, leading to different voltage changes. Therefore, the thermal conductivity of a tested sample can be obtained accurately by recording the change in voltage in a certain time period.

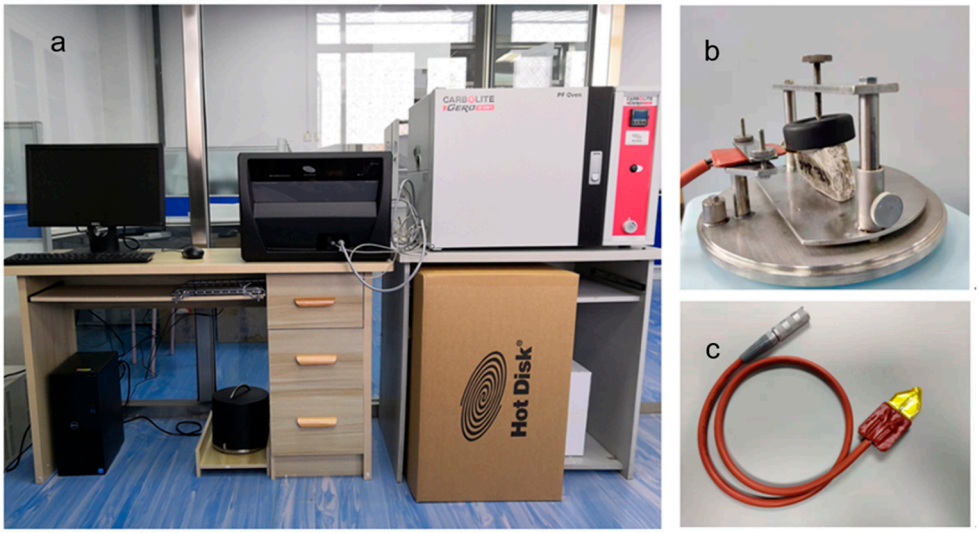

Figure 10. Schematic diagram of the thermal conductivity measurement principle: (**a**) Hot disk analyzer and the operating platform; (**b**) Testing of the rock samples according to the transient flat heat source method; (**c**) Thin-layer, disc-shaped probe.

The rock thermal conductivities in the Xiong'an New Area range 1.144–6.689 W/(m·K) with an average of 3.918 W/(m·K). Different lithologies exhibit different thermal conductivities, even for the same lithologic rocks. Clastic rocks vary from 1.144 to 2.687 W/(m·K), whereas carbonate data have a large variation from 1.6 to 6.689 W/(m·K). Dolomite, limestone, metamorphic rock, sandstone, magmatic rock, and mudstone exhibit mean thermal conductivities of 4.941, 3.453, 2.484, 1.814, 1.788, and 1.762 W/(m·K), respectively.

Several factors, such as temperature, pressure, porosity, and mineral composition, affect the rock thermal conductivity [32,33]. Different rocks exhibit different thermal conductivities due to the differences in mineral composition and structure. For the same rock types, mineral proportions and structures can vary, resulting in different thermal conductivities. The thermal conductivity decreases

with an increase in the temperature and increases with an increase in the pressure [34]. Pressure correction of the measured values was conducted using the thermal conductivity–pressure correction formula proposed by Sepold [35], and it was observed that the measured results exhibited a deviation of less than 1%; therefore, pressure correction [36] can be ignored. To a certain extent, the influence of temperature and pressure on the deep crust can offset each other [37]. Therefore, in this study, the effect of porosity on thermal conductivity was considered, whereas that on temperature or pressure was not considered.

Because air and water exhibit considerably different thermal conductivities, it is necessary to rectify the thermal conductivity of dry rocks evaluated in laboratory.

Based on previous research [38], the saturation correction was performed as follows:

$$K = K_m^{1-\Phi} \times K_w^{\Phi}, \tag{2}$$

where K is the corrected rock thermal conductivity W/(m·K), K_m is the thermal conductivity of the rock matrix W/(m·K), K_w is the thermal conductivity of water in the pores by considering 0.6 W/(m·K), and Φ is the porosity.

The strata in the Xiong'an New Area are mainly Cenozoic, Early Paleozoic, Proterozoic, and Archaean. The Cenozoic strata are shallowly deposited, and the sandstone porosity is large; therefore, water saturation correction is needed. The diagenesis of Paleozoic strata and the underlying strata in the Jizhong Depression is complex, and compaction can be observed throughout the diagenesis process [37]. The Proterozoic carbonate reservoir is characterized by complex diagenesis and strong heterogeneity, whereas pore space is mainly characterized by fissures and karst caves [11]. For the single sample characterized by low-to-ultralow permeability observed in the laboratory, it is difficult to determine the overall fracture development characteristics; therefore, thermal conductivity correction is not required. In the study area, mainly thermal conductivity correction of the Cenozoic sandstone samples was conducted.

The porosity correction of the Cenozoic sandstone thermal conductivity was performed (Table 1) according to (2). The correction coefficient is the ratio of the corrected thermal conductivity of the saturated rock samples to the measured thermal conductivity of the dry rock samples. Based on previous experiments [6,12], the saturation correction coefficients are mostly between 1.1 and 1.4, whereas those of the Cenozoic sandstone data obtained by the author are between 1.1 and 1.5 (Table 1), which are consistent with the previous research results.

Table 1. Calibration table of the thermal conductivity of Cenozoic sandstone rocks.

Serial Number	Sampling Location	Strata	Lithology	Thermal Conductivity W/(m·K)	Porosity (%)	Correction of Thermal Conductivity W/(m·K)	Correction Coefficient
1	C306	Ed	sandstone	1.433	7.5	1.863	1.30
2	G11	Es_1	sandstone	1.549	7	1.937	1.25
3	M14	Es_2	sandstone	1.79	12	2.609	1.46
4	M34	Es_1	sandstone	1.851	5	2.176	1.18
5	ND102	Es_4	sandstone	1.43	7.5	1.82	1.27
6	Xl12	Ng	sandstone	1.319	10.5	1.846	1.40
7	Y60	Es_2	sandstone	2.58	3	3.201	1.24
8	Y61	Es_1	sandstone	2.175	5	2.376	1.09
9	Y63	Es_1	sandstone	1.664	10	1.959	1.18
10	Y66	Es_2	sandstone	2.138	10	2.923	1.37

The corrected thermal conductivity was generally between 1.169 and 6.689 W/m K. The accuracy of hot disk analyzer measurement was high, and the data error was small at approximately 10^{-4}. Therefore, we plotted the analyzer measurement error of only 3% and mapped the distribution of the thermal conductivity. The relationship between the thermal conductivity and depth of main lithology is shown in Figure 11. Due to lack of data, no obvious relationship was observed between

the thermal conductivity and depth of sandstone and carbonate rocks. The relationship between the thermal conductivity and depth of different lithologies shown in Figure 12 demonstrates an obvious increasing trend in the thermal conductivity of clastic and metamorphic rocks with an increase in the depth, whereas the carbonate rock thermal conductivity shows no obvious change with depth and is relatively dispersed. The Proterozoic and Cenozoic strata in the North China Basin underwent complex tectonic evolution.

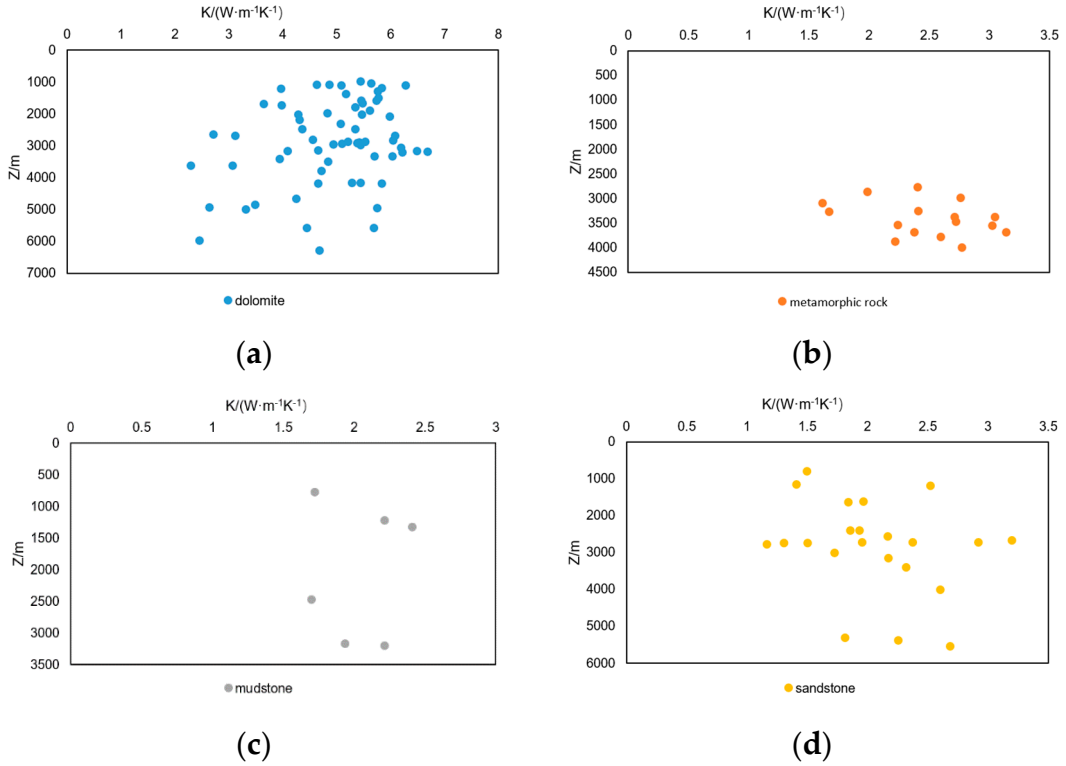

Figure 11. Relationship between thermal conductivity and depth of main lithologies. Relationship between dolomite and depth (**a**); Relationship between metamorphic rock and depth (**b**); Relationship between mudstone and depth (**c**); Relationship between sandstone and depth (**d**).

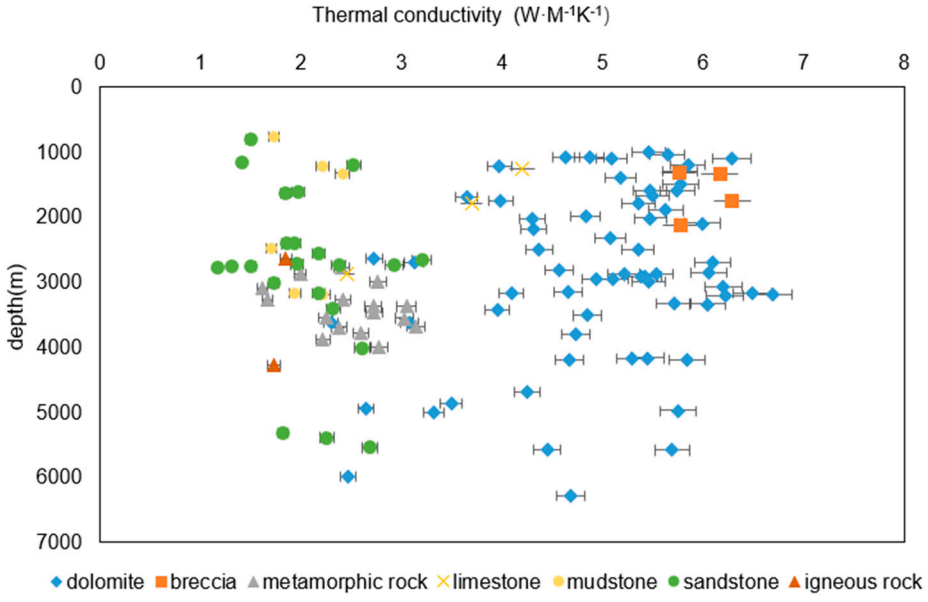

Figure 12. Relationship between the thermal conductivity and depth of different lithologies.

Since various regions contain different rock types and stratigraphic ages, the rock thermal conductivity treatment methods used in these regions differ. For areas exhibiting only one lithology, the arithmetic average value of thermal conductivity can be obtained. However, for areas exhibiting multiple lithologies, weighted or harmonic mean values are usually obtained. The harmonic average thermal conductivity can accurately represent thermal conductivity characteristics in the study area and is calculated as follows:

$$K = \frac{\Sigma di}{\Sigma \frac{di}{Ki}} = \frac{D}{\Sigma \frac{di}{Ki}}, \quad (3)$$

where di is the lithostratigraphic thickness of sample i (m), Ki is the thermal conductivity of sample i (W/(m·K)), and D is the thickness of the calculation interval (m).

Based on the thermal conductivity data of different lithologies in the Xiong'an New Area and the published thermal conductivity data for the Changjian and Leixiaodong [18,34], thermal conductivities were sorted by age and lithology, and the harmonic mean value of thermal conductivity average was calculated on the basis of the lithologic thickness of strata collected in different ages.

In Table 2, the rock thermal conductivity column in the Xiong'an New Area is listed as a basis for the geothermal heat flow calculation.

Table 2. Rock thermal conductivity column in the Xiong'an New Area.

Strata	Lithology	Number	Thermal Conductivity Range	Mean Value ± Standard Deviation	Harmonic Mean Value of Thermal Conductivity
Cenzoic (E + N)	Sandstone	18	1.169–3.201	2.016 ± 0.5197	2.006
	Mudstone	7	1.726–2.414	2.000 ± 0.2776	
	Limestone	2	2.108–4.2	3.154 ± 1.0458	
	Breccia	5	5.762–6.292	5.998 ± 0.2355	
Lower Palaeozoic (Pz)	Dolomite	3	3.975–5.081	4.336 ± 0.526	3.395
	Limestone	1	3.700	3.700	
	Mudstone *	13 *	1.836–3.590	2.869 ± 0.427	
Upper Proterozoic (Pt_3)	Mudstone	1	2.215	2.215	2.846
	Siltstone *	5 *	1.934–3.189	2.465 ± 0.524	
	Marlite *	10 *	2.449–3.792	3.309 ± 0.500	
Middle Proterozoic Jixianian (Pt_2)	Dolomite	46	2.466–6.689	5.155 ± 0.940	5.155
Middle Proterozoic Chang cheng System (Pt_2)	Quartz sandstone	1	2.687	2.687	4.361
	Sandstone	1	2.109	2.109	
	Dolomite	13	2.647–5.990	4.405 ± 0.986	
	Igneous rock	1	1.729	1.729	
	Limestone *	5 *	3.348–4.476	3.946 ± 0.491	
Archaean (Ar)	Gneiss	10	1.67–3.049	2.698 ± 0.758	2.661
	Granulite	7	1.617–3.143	2.479 ± 0.499	
	Igneous rock	1	1.848	1.848	

The * measurements were collected from lei et al. [34] and Chang et al. [18].

Owing to the thermal convection in the reservoir, only the heat flow in the caprock of the study area was studied.

Different heat flow calculation methods were used for different temperature-measurement data. To calculate the geothermal heat flow using systematic temperature data, the following mathematical expression was used:

$$q = G \cdot K, \quad (4)$$

where q denotes the geothermal flow (mW·m^{-2}), G denotes the geothermal gradient value of the thermometric interval (°C/Km), and K represents the corresponding layer's harmonic mean value of thermal conductivity (W/m·K).

The subsection method was used to calculate the geothermal flow for the temperature measurement wells. In this method, the average geothermal gradient is multiplied with the average thermal conductivity of the corresponding intervals. The rock thermal conductivity of the corresponding intervals was calculated using the harmonic average method (3), and the geothermal gradient was calculated using the least-squares method.

The thermal resistance method proposed by Chapman was adopted for the oil-testing data; the geothermal heat flow obtained by this method is expressed as follows:

$$q = \frac{Ts - To}{\sum_{i=0}^{n} \Delta Zi/Ki}, \quad (5)$$

where q is the geothermal flow (mW·m^{-2}), ΔZi is the difference in interlayer depth between adjacent structures, Ki is the formation thermal conductivity at a depth of Zi (W/m·K), Ts is the temperature data of oil testing, and To is the constant temperature zone (14 °C).

Based on the previously collected geothermal gradient data and corresponding rock thermal conductivity, the geothermal flow of 105 wells was calculated in the study area and planar distribution map of the geothermal heat flow in the Xiong'an New Area was obtained (Figure 13).

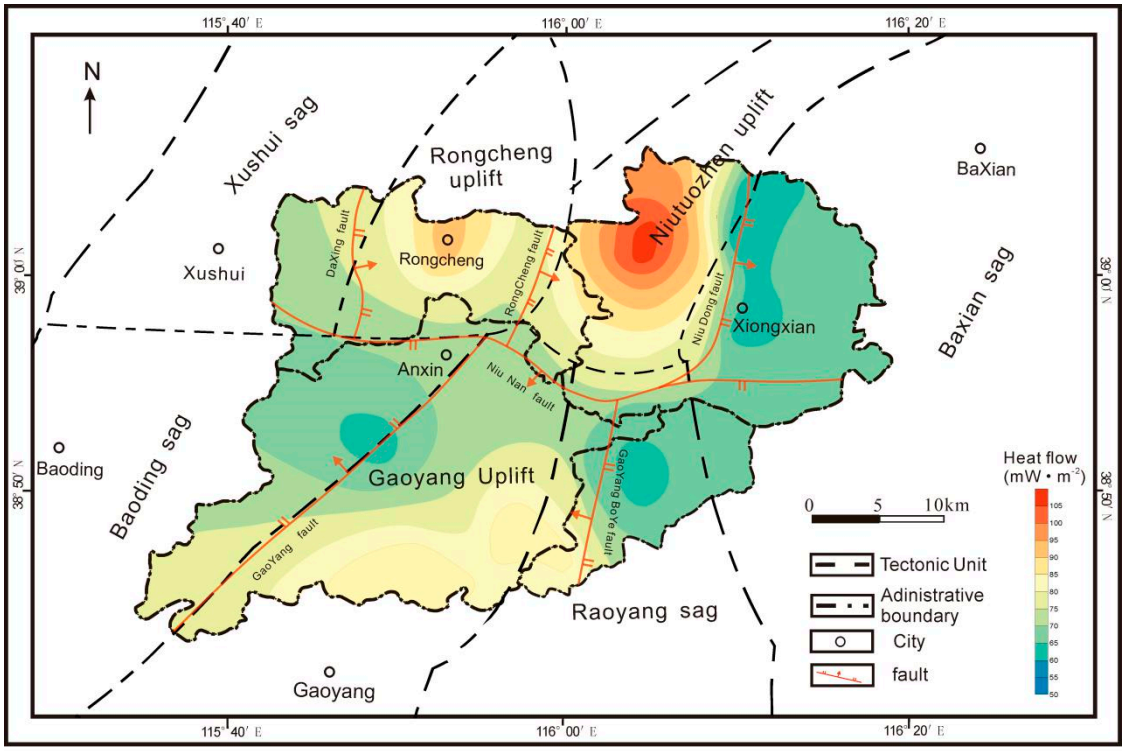

Figure 13. Geothermal heat flow distribution map of the Xiong'an New Area.

The overall geothermal flow in the Xiong'an New Area is 53.3–106.5 mW·m^{-2}, which belong to the high anomaly area with an average of 73 mW·m^{-2}. The mean heat flow in the mainland of China is 63 ± 24.2 mW·m^{-2}, the value is 56.54 mW·m^{-2} [39] in the southern part of the North China Craton and 69 mW·m^{-2} in the Bohai Bay Basin, which are all lower than the value in the study area.

The heat flow in the North China Craton is relatively high than that in other cratons in the world. The present geothermal characteristics result from basin thermal evolution is closely related to tectonic evolution. After the Mesozoic, North China underwent craton destruction and lithospheric thinning

events, which were important tectonic events affecting the geothermal heat flow, providing the study area with a high background heat flow [32,40].

4. Main Factors Affecting the Geothermal Temperature Field

Geothermal anomalies are the consequence of the interplay between a range of geological and hydrological conditions. In the Xiong'an New Area these controlling conditions are the basement structure, large faults, and groundwater factors, leading to present geothermal field characteristics.

By analyzing the geological characteristics and rock properties of the reservoirs and caprocks and observing the logging curve (Figure 14), the porosity of the caprocks was found to be high because it is mainly dominated by sand and mudstone. Thermal reservoirs, especially the reservoir in the uplifts, always have multiple fracture zones. When fractures develop well in the reservoir, the porosity becomes high, indicating that the gamma logging curve shows a high value that even exceeds that of the caprocks. Based on the above characteristics, we inferred that the migration path of groundwater tends to upward to geothermal reservoirs (Figure 15).

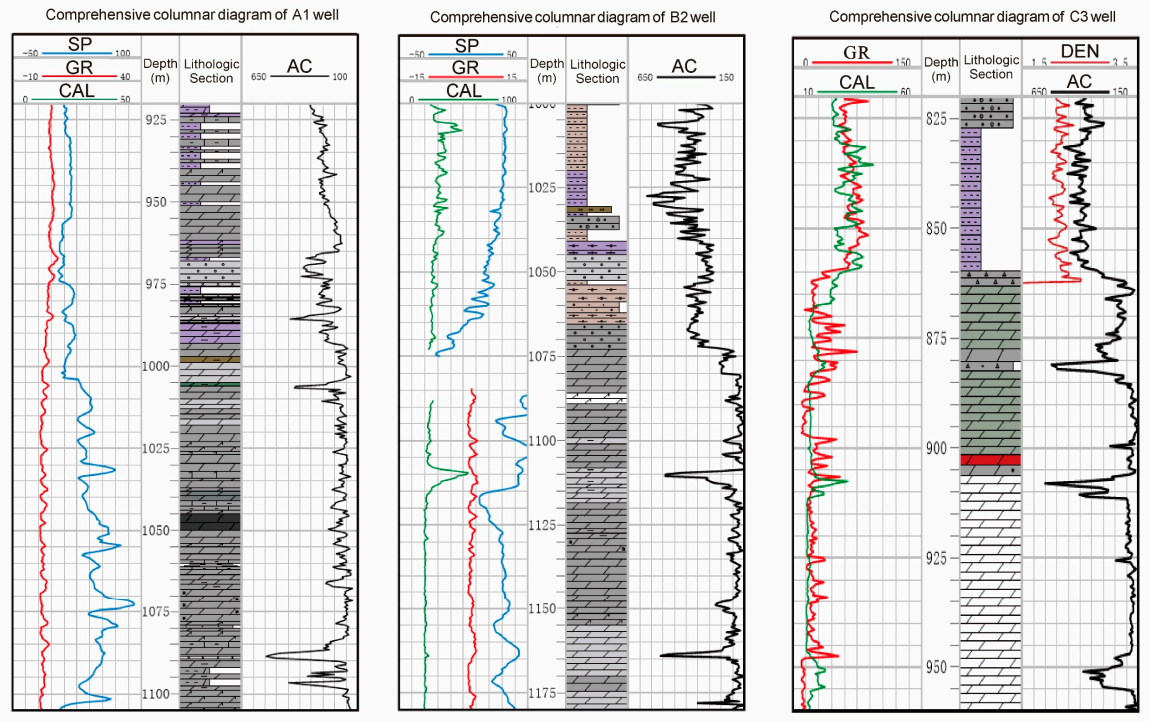

Figure 14. Comprehensive columnar diagram of typical wells in the Xiong'an New Area. (**a**) Comprehensive columnar diagram of A1 well; (**b**) Comprehensive columnar diagram of B2 well; (**c**) Comprehensive columnar diagram of C3 well.

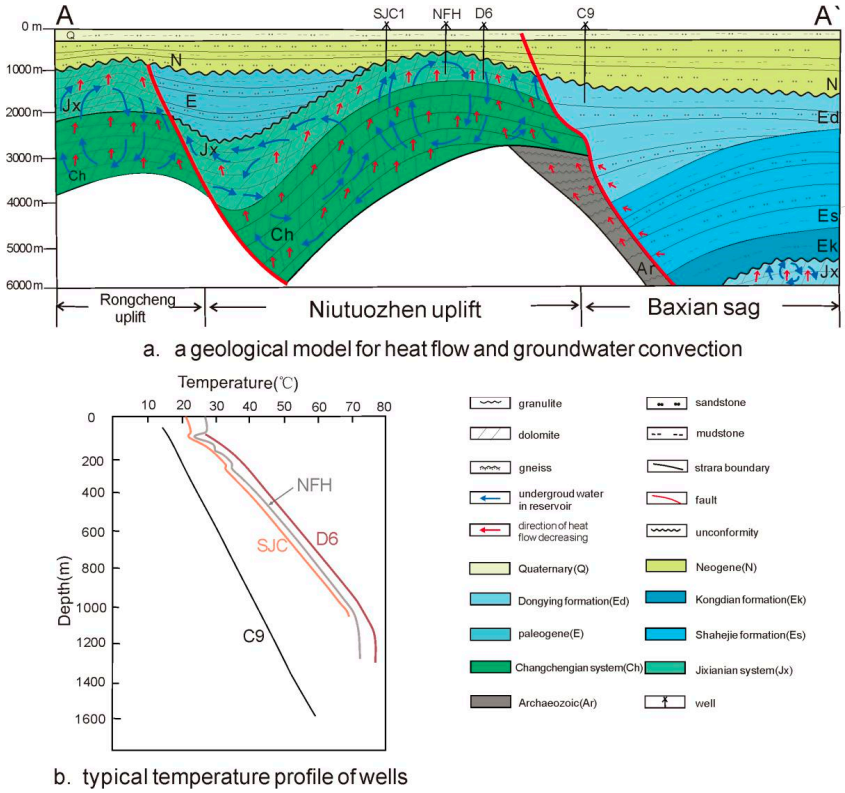

Figure 15. Geological model for heat flow and groundwater convection in section AA′ (for location, see Figure 2a) of the Xiong'an New Area. A geological model for heat flow and groundwater convenction (**a**); Typical temperature profile of wells (**b**) C9 well is in Baxian sag and NFH1, SJC1, and D6 well are in Niutuozhen uplift. Temperature profile of typical wells provides evidence to the temperature distribution model.

4.1. Basement Structure

Basement relief and tectonic configuration dominate the geothermal field distribution in the shallow crust [41]. The geotemperature and geothermal gradient distribution in the area are obviously related to the basement structure and thickness of the sedimentary caprock.

Due to the different structural configurations in uplifts and sags, the rock thermal conductivity changes in the horizontal and vertical directions, resulting in terrestrial heat flow redistribution, where uplifts have high heat flow values and sags have low heat flow values [6,42].

As shown in Figure 13, the uplift geothermal flow in the Xiong'an New Area is relatively high, with the heat flow value in the core area of the Niutuozhen uplift up to 106.5 $mW{\cdot}m^{-2}$, followed by up to 90 and 87.2 $mW{\cdot}m^{-2}$ in the Rongcheng and Gaoyang uplift, respectively. When compared with the heat flow values in the uplifts, those in the sags are relatively low. Particularly, the heat flow in the Baxian and Raoyang sag is between 48.9 and 61.6 $mW{\cdot}m^{-2}$ and 53.3 and 65.7 $mW{\cdot}m^{-2}$, respectively.

Different thermal conductivities of rocks in different strata lead to geothermal gradient changes in the longitudinal direction and cause the convergence of lateral heat flow from low to high thermal conductivity. Therefore, the differences in thermal conductivity of the Cenozoic caprock, Proterozoic carbonate rock geothermal reservoir, and basement cause the redistribution of heat flow to the surface during conduction, i.e., heat flow concentrates in the thin uplift area, resulting in lower geothermal temperatures in sags than in uplifts as well as a geotemperature difference in map view [43,44].

The uplift geothermal gradients are generally higher than the depression area geothermal gradients because depressions have thicker sedimentary layers, mainly comprising sandstone, mudstone, and thicker caprock. Therefore, the thermal conductivity is low, causing a shielding effect on heat from the

deep crust. However, the caprock thickness in the uplifts is relatively low, and the basement rock is dominated by the Jxw Formation dolomite, which exhibits considerable thermal conductivity.

Zhou et al. [17] found that the isotherm of the upper part of uplift is a convex curve, which is consistent with the basement relief. On the contrary, the lower part of the isotherm in a sag is a concave curve. A horizontal isotherm exists between the convex and concave curves. Heat flow below the horizontal isotherm is concentrated from the sag to the uplift, whereas it diverges outward near the vertical interface above the horizontal isotherm and converges to the high part of the uplift (Figure 15).

4.2. Fractures

A coupling relationship exists between the geothermal field distribution and fractures. The existence of faults not only act as heat flow barriers but also cause the transfer and migration of heat flow. Therefore, high and low abnormal heat flows often occur near large faults (Figure 13) [5].

Different fracture systems exhibit complex evolutionary histories that control the tectonic deformation and evolution of the area. The area developed the NE, NNE, and SW faults, with the NNE fault being the most developed. The faults, mostly normal and strike-slip faults, are large and deep. The secondary tectonic units are mainly controlled by deep and large faults. The geotemperature and geothermal gradient mainly extend to the NNE and NE. The high geothermal field is distributed along the tectonic trend; the high value is consistent with the structural high point and closely related to the large fault.

The Niudong fault is between the Niutuozhen uplift and Baxian sag (Figure 15). The Niudong fault is a high-angle extensional normal fault with large drop and strong activity, and it is the main channel for groundwater activity [11]. Therefore, a high heat flow area is formed in the Niutuozhen uplift.

The east side of the Rongcheng uplift is the Rongcheng fault, which has a NNE strike and dip angle of approximately 45°, making it gentler than Niudong fault. The vertical displacement of the Rongcheng fault is up to 3000 m, which makes it a growing fault that controls the development of the Neogene formation [45]. Based on the gravity anomaly characteristic analysis, previous studies found that the Rongcheng fault is an upwelling exit of the hot water in the Niuzuozhen basement rock and produces many crack zones and dissolution zones [46].

4.3. Groundwater Activity

Heat transfer mainly occurs though conduction in the Cenozoic caprock and convection in the Proterozoic geothermal reservoir. By analyzing the hydrochemistry and isotope geochemistry, Zhou et al. [17] determined that groundwater in the area originated from the Taihang and Yanshan mountains to the west and north, respectively. The groundwater supply is mainly dependent on atmospheric precipitation, which can be determined by the hydrogen and oxygen isotope data lines near the meteoric water line [47]. Furthermore, strong activity was observed in the Quaternary and Upper Tertiary.

The surface water penetrates deep along the Niudong and Rongcheng faults, becoming high-temperature water after being heated by the deep heat sources. The Niudong fault is a heat-controlling fault, with an overall NNE strike. With favorable vertical groundwater connectivity and large circulation depth, the Niudong fault plays an obvious role in controlling the Niutuozhen uplift's geothermal field.

The bottom of some temperature–depth curves near the Niudong fault zone show obvious convex forms, indicating an upwelling fissure with high-temperature water. The rNa/rCl ratio of the Jxw Formation in the Niutuozhen uplift is greater than 1.0 and mineralization degree is less than 30 g/L, indicating $NaHCO_3$-type formation water with a relatively open environment. The rNa/rCl ratio of the Quaternary formation water in the Baxian sag is less than 1.0 and mineralization degree is greater than 40 g/L, indicating $CaCl_2$-type formation water in a relatively closed environment [43]. Furthermore, the groundwater quality in the geothermal reservoirs of the uplift and lower sag is significantly different, demonstrating that the Niutuozhen uplift exhibits high geotemperature, large

groundwater circulation depth, and good vertical connectivity. Besides, according to the quartz geothermometers, the previous calculated the temperatures for Jxw reservoirs ranging from 81 °C to 127 °C [48]. Moreover, the groundwater temperature is significantly different from that of the Baxian sag, indicating poor horizontal connectivity [17,49].

The Rongcheng fault shows peculiarity with respect to the conducting water. High-temperature groundwater upwells along the fault, causing high geotemperature in the Rongdong buried hill. However, the Rongcheng uplift's geothermal gradient is lower than that of the Niutuozhen uplift, which may be closer to the groundwater recharge area and is affected by cold water [11].

Combined with the Jxw Formation's top temperature (Figure 9), the top temperature of the geothermal reservoir in the Niutuozhen and Rongcheng uplifts is less than that of the Baxian sag. It may be that deep hot water loss heat moving upward along the Niudong fault or that hot water merges with shallow cold water, reducing the temperature.

Studies based on the deep geothermal fields relies on understanding of shallow geothermal fields, provided that the structure of the area is relatively stable and that the temperature field is in a steady state [50]. Zhou et al. and Chang et al. [17,18] noted an abnormally high heat flow caused by groundwater and determined that it could not reflect the area's heat flow state. Therefore, some wells with abnormal values were excluded from the heat flow study.

5. Discussion

The Xiong'an New Area is rich in geothermal resources with large geothermal reservoir area and high temperature. It is a demonstration area for the development and utilization of medium–low temperature geothermal energy in China. Xiongxian, a typical geothermal field, has used the geothermal reservoir to provide large-scale heating. This study on the geothermal resources in the Xiong'an New Area was performed to mainly clarify the geothermal and geological conditions, namely the characteristics of the heat source, thermal reservoir, caprocks, and channels. The heat in the area mainly comes from the radioactive elements in the upper crust and is generated by the upper mantle. The water source is mainly supplied by meteoric precipitation, and the underground cold water upwelling along the deep and large faults after heating. Then, it accumulates in the Proterozoic carbonate thermal reservoirs, and Cenozoic caprocks provide favorable heat accumulation conditions. In addition, prior researchers estimated the resources in the Xiong'an New Area.

Li et al. estimated the maximum temperature of the carbonate thermal reservoir to reach 225 °C on the basis of the measured temperature curve for the Xiong'an New Area. The volume and Monte Carlo methods were used to calculate the hydrothermal geothermal resources above 40 °C in the area, including the hot water reserves of the Neogene and Archaeozoic reservoirs. The thermal storage capacity of the carbonate thermal reservoir in Xiong'an New Area is $14.5 \pm 5.4 \times 10^{16}$ kJ, which is equivalent to 49.6 ± 1.86 billion tons of standard coal. At the recovery rate of 15%, recoverable heat is $2.2 \pm 0.8 \times 10^{16}$ kJ, which is equivalent to 7.4 ± 280 million tons of standard coal. The heat for hot water was found to be $1.4 \pm 0.8 \times 10^{16}$ kJ, which is equivalent to 4.7 ± 280 million tons of standard coal [14]. Wang et al. mapped the temperature contour diagram of the middle depth within the Proterozoic geothermal reservoir and found that the maximum temperature of middle depth was up to 118 °C. The minimum and maximum values for geothermal resources in the Xiong'an New Area were calculated using the volume method because the parameters were uncertain. The minimum and maximum values of heat storage in the carbonate thermal reservoir were found to be 35.6×10^{16} and 297.9×10^{18} kJ, which is equivalent to a heat content of approximately 10 billion tons of coal [19].

Previous studies on the Xiong'an geothermal resources adopted the volume method. The influence of the physical rock properties and other parameters was considered in calculations, whereas that of groundwater activity on the geothermal field was not considered. Due to the influence of groundwater activities, the actual reservoir heat storage is likely less than the calculated value.

Well drilling in the area was mainly focused on uplift and the drilling strata were focused on the Paleozoic sandstone formation. Most wells were oil wells, and there is lack of geothermal wells,

especially deep geothermal wells. Due to the drilling conditions, we could not obtain real steady-state heat flow data. Therefore, to determine the amount of groundwater activity that affects the geothermal field, temperature measurements of deep wells are required. Determining the temperature in the metamorphic basement, which is not affected by convection under the Jxw reservoir, would play an important role in understanding the deep conductive geothermal field in the Xiong'an New Area.

6. Conclusions

1. The geothermal gradient in the Xiong'an New Area is 24.6–72.8 °C/km, with an average of 35 °C/km, which is consistent with the basement relief over the region. In addition, the logging data indicate that the geothermal gradient is higher in uplifts (average value of 40 °C/km) and lower in depression areas (average value of 30 °C/km). The top surface temperature of the Jxw reservoir shows that the temperatures in the north and northwest are low, whereas that of the southeast is high.
2. The thermal conductivities of different lithologies range 1.144–6.689 W/m·K. The average thermal conductivities, ranked from high to low, were dolomite (4.941 W/(m·K)), limestone (3.453 W/(m·K)), metamorphic rock (2.484 W/(m·K)), sandstone (1.814 W/(m·K)), igneous rock (1.788 W/(m·K)), and mudstone (1.762 W/(m·K)). The harmonic average thermal conductivity of each layer was calculated on the basis of the lithological ratio, with the Cenzoic strata mainly comprising sandstone and mudstone with an average thermal conductivity of 2.006 W/(m·K); the early Paleozoic strata mainly comprising limestone and mudstone with an average thermal conductivity of 3.395 W/(m·K); the early and middle Proterozoic dominated by dolomite with average thermal conductivities of 4.361 and 5.155 W/(m·K), respectively; late Proterozoic dominated by marl with an average thermal conductivity of 2.846 W/(m·K); and Archaean dominated by granulite and gneiss with an average thermal conductivity of 2.661 W/(m·K).
3. The terrestrial heat flow in the Xiong'an New Area is 53.3–106.5 $mW \cdot m^{-2}$, with an average of 73 $mW \cdot m^{-2}$, which is higher than mainland China's average value of 63.0 ± 24.2 $mW \cdot m^{-2}$. This resulted from the destruction of the North China Craton. Regionally, geothermal flow is obviously controlled by the basement structure, with higher heat flow in uplifts and lower heat flow in sags.
4. The present geothermal field in the Xiong'an New Area is mainly controlled by an interphased uplift and sag tectonic pattern. Under this tectonic setting, heat flow redistributed to the surface and converged in uplifts during conduction because of the lower thermal conductivity in caprocks and higher thermal conductivity in reservoirs and basement rocks. Furthermore, the groundwater activity through faults and convection in geothermal reservoirs is important for forming high-temperature groundwater. Under the influence of complex tectonic settings and groundwater activity, the area's geotemperature has been redistributed from deep to shallow, and the measured heat flow in shallow caprocks cannot reflect the deep thermal state.

Author Contributions: Conceptualization, S.G. and C.Z.; Methodology, S.G. and C.Z.; Software, S.G.; Validation, C.Z. and N.Q.; Formal Analysis, S.G.; Investigation, S.G., B.T., J.Z. and Y.C.; Resources, S.G., C.Z. and N.Q.; Data Curation, S.G., B.T. and Y.C.; Writing-Original Draft Preparation, S.G.; Writing-Review & Editing, C.Z.; Visualization, S.G. and Y.Z.; Supervision, N.Q.; Project Administration, C.Z. and N.Q.; Funding Acquisition, C.Z. and N.Q.

Funding: This research was funded by the National key research and development program of China (Grant No. 2018YFC0604302), the Beijing Training Project of Science and Technology Nova and Leading Talent (Grant No. Z171100001117163). We are grateful to the Institute of Hydrogeology Environmental Geology, Chinese Academy of Geological Sciences for providing research data and rock samples.

Conflicts of Interest: The authors declare no conflicts of interest.

Nomenclature

Φ	Porosity [%]
K	Thermal conductivity [W/(m·K)]
D	Thickness [m]
G	Geothermal gradient [°C/km]
Z	Depth [m]
T	Temperature [°C]
q	Heat flow [mW·m^{-2}]

References

1. Rao, S.; Jiang, G.; Gao, Y.; Hu, S.; Wang, J. The thermal structure of the lithosphere and heat source mechanism of geothermal field in Weihe Basin. *Chin. J. Geophys.* **2016**, *59*, 2176–2190.
2. Tang, X.; Huang, S.; Yang, S.; Jiang, G.; Hu, S. Correcting on logging-derived temperatures of the Pearl River Mouth Basin and characteristics of its present temperature field. *Chin. J. Geophys.* **2016**, *59*, 2911–2921.
3. Zhang, X.; Gu, Y.; Shao, Z.; You, D.; Ding, Y.; Wan, Y. Control effect of geothermal field on hydrocarbon accumulation process in Tarim Basin: A case study of Guchengdu uplift. *Acta Pet. Sin.* **2017**, *38*, 502–511.
4. Jaupart, C.; Labrosse, S.; Lucazeau, F.; Mareschal, J.C. 7.06—Temperatures, Heat, and Energy in the Mantle of the Earth. *Treatise Geophys.* **2015**, *7*, 223–270.
5. Rutledge, J.T.; Phillips, W.S.; Mayerhofer, M.J. Faulting induced by forced fluid injection and fluid flow forced by faulting: An interpretation of hydraulic-fracture microseismicity, Carthage Cotton Valley Gas Field, Texas. *Bull. Seismol. Soc. Am.* **2004**, *94*, 1817–1830. [CrossRef]
6. Xiong, L.; Gao, W. Characteristics of geotherm in uplift and depression. *Acta Geophys. Sin.* **1982**, *5*, 60–68.
7. Xiong, L.; Zhang, J. Relationship between geothermal gradient and the relief of basement rock in North China plain. *Acta Geophys. Sin.* **1988**, *2*, 146–155.
8. Gong, Y.; Wang, L.; Liu, S.; Li, C.; Han, Y.; Li, H.; Liu, B.; Cai, J. Distribution Characteristics of Terrestrial Heat Flow in the Jiyang depression. *Sci. China (Ser. D)* **2003**, *4*, 384–391.
9. Li, Z.; Gao, J.; Li, W.; Wu, J.; Liu, C.; Ma, Y. The characteristics of geothermal field and controlling factors in Qaidam Basin, Northwest China. *Earth Sci. Front.* **2016**, *23*, 23–32.
10. Hu, S.; Xiong, L. Correction for disturbance of vertical groundwater movement to heat flow measurement. *Sci. Geol. Sin.* **1994**, *1*, 85–92.
11. Chen, M.; Huang, G.; Zhang, W.; Zhang, R.; Liu, B. The Temperature Distribution Pattern and the Utilization of Geothermal Water at Niutuozhen Basement Protrusion of Central Hebei Province. *Sci. Geol. Sin.* **1982**, *3*, 239–252.
12. Chen, M.; Wang, J.; Wang, J.; Deng, X.; Yang, S.; Xiong, L.; Zhang, J. The Characteristics of the Geothermal Field and its Formation Mechanism in the North China Down-faulted Basin. *Acta Geol. Sin.* **1990**, *1*, 80–91.
13. Sun, A.; Niu, S. The Mantle Plume Evolution and Its Geothermal Effect Deep Tectonic Setting of Geothermal Anomaly in North China. *Acta Geosci. Sin.* **2000**, *2*, 182–189.
14. Li, W.; Rao, S.; Tang, X. Borehole temperature logging and temperature field in the Xiongxian geothermal, Hebei Province. *Chin. J. Geol.* **2014**, *49*, 850–863.
15. Wang, Y.; Ding, W.; Tian, Y.; Wang, J.; Ding, R. Genetic Analysis on High-temperature Geothermal Water in Niutuo Geothermal Field, Heibei Province. *Urban Geol.* **2016**, *11*, 59–64.
16. Lv, C. Characteristics and genetic mechanism of geothermal system in the geothermal field of Niu Tuo Town. *Ground Water* **2018**, *40*, 28–30.
17. Zhou, R. The activity of deep underground water in the northern part of the north China plain and its effect on the geothermal field. *Bull. Brig. Chin. Acad. Geol. Sci.* **1987**, *6*, 17–35.
18. Chang, J.; Qiu, N.; Zhao, X.; Xu, W.; Xu, Q.; Jin, F.; Han, C.; Ma, X.; Dong, X.; Ling, X. Present-day geothermal regime of the Jizhong depression in Bohai Bay Basin, East China. *Chin. J. Geophys.* **2016**, *59*, 1003–1016.
19. Wang, Z.; Jiang, G.; Zhang, C.; Hu, J.; Shi, Y.; Wang, Y.; Hu, S. Thermal regime of the lithosphere and geothermal potential in Xiong'an New Area. *Energ. Explor. Exploit.* **2018**, *37*, 787–810. [CrossRef]
20. Qiu, N.; Xu, W.; Zuo, Y.; Chang, J.; Liu, C. Evolution of meso-cenozoic thermal structure and thermal-rheological structure of the lithosphere in the bohai bay basin, eastern north china craton. *Earth Sci. Front.* **2017**, *51*, 794–804.

21. He, L.; Hu, S.; Wang, J. Thermal regime of the continental lithosphere in the eastern China. *Prog. Nat. Sci.* **2001**, *9*, 72–75.
22. Jiang, G.; Gao, P.; Rao, S.; Zhang, L.; Tang, X.; Huang, F.; Zhao, P.; Pang, Z.; He, L.; Hu, S.; et al. Compilation of heat flow data in the continental area of China (4th edition). *Chin. J. Geophys.* **2016**, *59*, 2892–2910.
23. Zhang, Y.; Chang, J.; Liu, N.; Liu, J.; Ma, X.; Zhao, F.; Zhou, Y. Present-day temperature–pressure field and its implications for the geothermal resources development in the Baxian area, Jizhong Depression of the Bohai Bay Basin. *Nat. Gas Ind.* **2017**, *37*, 118–126. [CrossRef]
24. Dai, F.; Liu, B.; Yang, K. Geological interpretation of seismic sections and tectonic evolution of the North China basin. *Geol. China* **2008**, *35*, 820–840.
25. Wang, J.; Wang, J.; Shen, J.; Qiu, N. Heat Flow in Tarim Basin. *Earth Sci.-J. China Univ. Geosci.* **1995**, *4*, 399–404.
26. Lin, S.; Gong, Y. Distribution Charaterisitcs of GeotemPerature Field in Jizhong DePression, North China. *J. East China Inst. Technol.* **2005**, *4*, 359–364.
27. Yuan, Y.; Hu, S.; Wang, H.; Sun, F. Meso-Cenozoic tectonothermal evolution of Ordos basin, central China: Insights from newly acquired vitrinite reflectance data and a revision of existing paleothermal indicator data. *J. Geodyn.* **2007**, *44*, 33–46. [CrossRef]
28. Wang, L.; Li, C.; Liu, S.; Li, H.; Xu, M.; Wang, Q.; Ge, R.; Jia, C.; Wei, G. Geotemperature Gradient Distribution of Kuqa Foreland Basin, North of Tarim, China. *Chin. J. Geophys.* **2003**, *46*, 403–407. [CrossRef]
29. Majorowicz, J.; Grasby, S.E. Heat flow, depth-temperature variations and stored thermal energy for enhanced geothermal systems in Canada. *J. Geophys. Eng.* **2010**, *7*, 232. [CrossRef]
30. Panel, M.L. The Future of Geothermal Energy. Impact of Enhanced Geothermal Systems [EGS] on the United States in the 21st century. *Geothermics* **2006**, *17*, 881–882.
31. Liu, S.; Li, X.; Hao, X.; Li, X. Heat flow, deep formation temperature and thermal structure of the Tarim Basin, Northwest China. *Earth Sci. Front.* **2017**, *24*, 041–055.
32. Xu, M.; Zhu, C.; Tian, Y.; Rao, S.; Hu, S. Borehole temperature logging and characteristics of subsurface temperature in the Sichuan Basin. *Chin. J. Geophys.* **2011**, *54*, 1052–1060. [CrossRef]
33. Clauser, C.; Huenges, E. Thermal Conductivity of Rocks and Minerals. In *Rock Physics and Phase Relations: A Handbook of Physical Constants*; American Geophysical Union: Washington, DC, USA, 1995; pp. 105–126.
34. Lei, X.; Hu, S.; Li, J.; Jiang, G.; Yang, Q.; Li, Q. Characteristics of heat flow and geothermal distribution in the northwest Beijing plain. *Chin. J. Geophys.* **2018**, *61*, 3735–3748.
35. Seipold, U. Pressure Dependence of Thermal Conductivity of Rocks. *High Press. Food Sci. Biosci. Chem.* **1998**, 474–480. [CrossRef]
36. Zhang, C.; Zhang, S.; Li, S.; Jia, X.; Jiang, G.; Gao, P.; Wang, Y.; Hu, S. Geothermal characteristics of the Qiabuqia geothermal area in the Gonghe basin, northeastern Tibetan. *Chin. J. Geophys.* **2018**, *61*, 4545–4557.
37. Zhou, L. Genetic Mechanism and Distribution Patterns of Medium-Deep High-Quality Clastic Reservoirs of Paleogene Jizhong Depression. Master's Thesis, East China University of Petroleum, Beijing, China, 2014.
38. Woodside, W.; Messmer, J.H. Thermal conductivity of porous media. Unconsolidated sands. *J. Appl. Phys.* **1961**, *32*, 1699–1706. [CrossRef]
39. He, Z.; Liu, C.; Zhao, J.; Liu, Y. A Study on Geothermal Field and Its Geological Significance in Southern Area of the North China Craton. *Geol. Rev.* **2009**, *55*, 428–434.
40. Feng, C.; Liu, S.; Wang, L.; Li, C. Heat flow, deep formation temperature and thermal structure of the Tarim Basin, Northwest China. *Earth Sci. Front.* **2009**, *52*, 2752–2762.
41. Liang, H.; Qian, Z.; Xin, S.; Zhao, K.; Zhu, L. Assessment and Development of Geothermal Resources in Jizhong Depression. *New Energy* **2010**, *15*, 63–68.
42. Lin, G.; Nunn, J.A.; Deming, D. Thermal buffering of sedimentary basins by basement rocks: Implications arising from numerical simulations. *Pet. Geosci.* **2000**, *6*, 299–307. [CrossRef]
43. Li, F.; Li, S.; Zeng, J.; Liu, J.; Liu, J.; Ge, D.; Wang, Y.; Mu, Y. Feature of Paleofluids and Present Fluids in the Inner Buried Hill of Niutuozhen Uplift, Baxian Sag. *Geoscience* **2016**, *30*, 1115–1123.
44. Wang, L.; Liu, S.; Xiao, W.; Li, C.; Li, H.; Guo, S.; Liu, B.; Luo, L.; Cai, D. Distribution Charaterisitcs of terrestrial heat flow in Bohai Bay Basin. *Sci. Bull.* **2002**, *47*, 151.
45. Wang, G.; Li, J.; Wu, A.; Zhang, W.; Hu, Q. A Study of the Thermal Storage Characteristics of Gaoyuzhuang Formation, A New Layer System of Thermal Reservoir in Rongcheng Uplift Area, Hebei Province. *Acta Geosci. Sin.* **2018**, *39*, 533–541.

46. Li, H.; Yu, J.; Lv, H.; Xiao, P. Gravity and aeromagnetic responses and heat-controlling structures of Xiongxian geothermal area. *Geophys. Geochem. Explor.* **2017**, *41*, 242–248.
47. Yang, J.; Liu, F.; Jia, Z.; Yuan, H.; Xu, Q.; Hu, Y. The Hydrochemical and δ2H-δ18O Characteristics of Two Geothermal Fields in Niutuozhen of Hebei Province and Tianjin and Their Environmental Significance. *Acta Geosci. Sin.* **2018**, *39*, 71–78.
48. Pang, J.; Pang, Z.; Lv, M.; Tian, J.; Kong, Y. Geochemical and isotopic characteristics of fluids in the niutuozhen geothermal field, north china. *Environ. Earth Sci.* **2018**, *77*, 12. [CrossRef]
49. Wang, Y.; Zhang, G.; Sun, B. Geologicaland geochemical characteristics of bedrock water and sensitivity for earthquake precursory in Niutuozhen. *Geol. Geochem.* **1994**, *5*, 69–72.
50. Zhi, J.; Du, J.; Chen, C. Characteristics of Large-Scale Thermal Structure in Lithosphere beneath Junggar Basin and Surroundings. *Earth Sci.* **2018**, *43*, 103–118.